Chapter 12

Doping-Induced Ferroelectric Phase Transition and Ultraviolet-Illumination Effect in a Quantum Paraelectric Material Studied by Coherent Phonon Spectroscopy

Toshiro Kohmoto

Additional information is available at the end of the chapter

http://dx.doi.org/10.5772/45744

1. Introduction

There has been significant interest in a quantum paraelectric material strontium titanate ($SrTiO_3$), and its lattice dynamics and unusual dielectric character have been extensively studied. In low temperatures, its dielectric constant increases up to about 30 000. The dielectric constant increases extraordinarily with decreasing temperature while the paraelectric phase is stabilized by quantum fluctuations without any ferroelectric phase transition even below the classical Curie temperature T_c=37 K [1]. In $SrTiO_3$, a ferroelectric transition is easily induced by a weak perturbation such as an uniaxial stress [2], an isotopic substitution of oxygen 18 for oxygen 16 [3], and an impurity doping [4,5].

$SrTiO_3$ has a perovskite structure as shown in Fig. 1(a) and is known to undergo a structural phase transition at T_c=105 K [6]. The cubic (O_h) structure above T_c, where all phonon modes are Raman forbidden, changes into the tetragonal (D_{4h}) structure below T_c, where Raman-allowed modes of symmetries A_{1g} and E_g appear [7]. The phase transition is due to the collapse of the Γ_{25} mode at the R point of the high-temperature cubic Brillouin zone. Below T_c, the R point becomes the Γ point of the D_{4h} phase. The phase transition is characterized by the softening of phonons at the R point and concomitant doubling of the unit cell.

The distortion consists of an out-of-phase rotation of adjacent oxygen octahedra in the (100) planes [6]. The order parameter for the phase transition is inferred to be the angle of rotation of the oxygen octahedra. Only a small rotation of the oxygen octahedra is involved for the transition. The rotation angle for the oxygen octahedra varies from ~2° of arc near 0 K down

to zero at T_c=105 K; the transition is second order. At liquid nitrogen temperature, the rotation angle is about 1. 4° and the linear displacement of the oxygen ions about their high-temperature equilibrium positions is less than 0.003 nm. This oxygen octahedron motion can be described as a rotation only as a first approximation; the oxygen ions actually remain on the faces of each cube and therefore increase in separation from the titanium. Because the (100) planes are equivalent in the cubic phase, the distortion produces domains below *Tc* in which the [100], [010], or [001] axis becomes the unique tetragonal *c* axis.

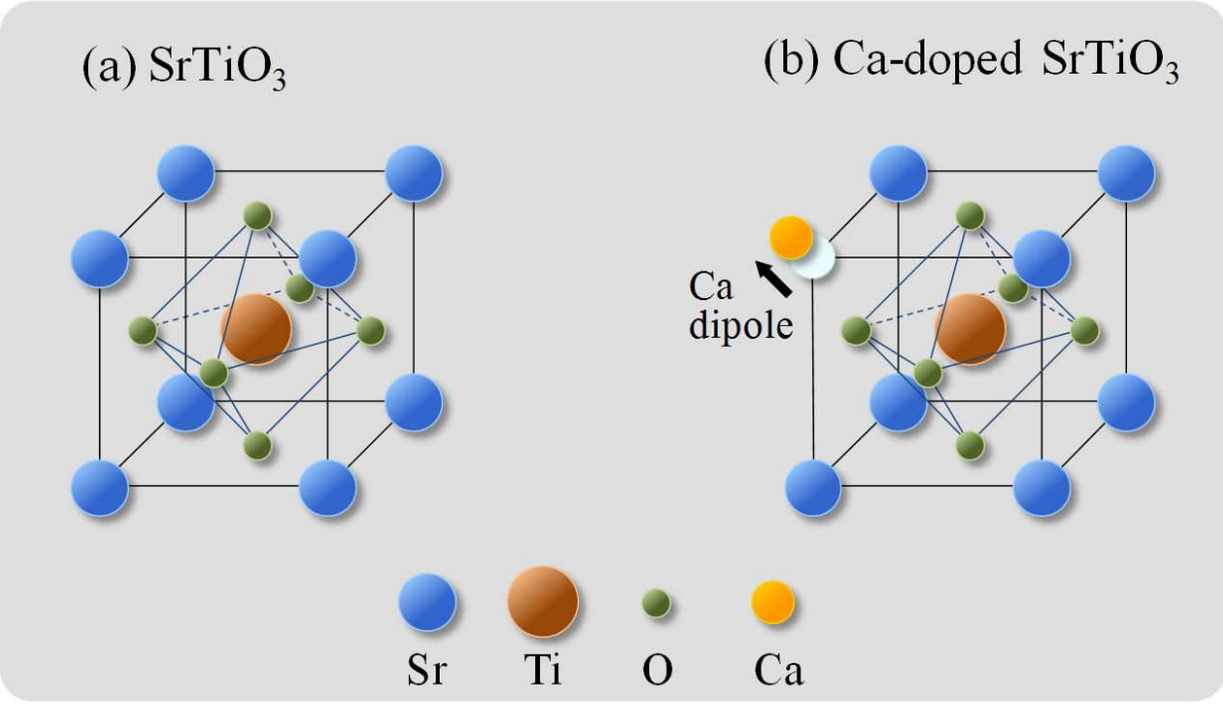

Figure 1. (a) Perovskite structure in $SrTiO_3$. (b) Doped Ca ions are substituted for the Sr ions in Ca-doped $SrTiO_3$.

According to the measurement of dielectric constants, $Sr_{1-x}Ca_xTiO_3$ undergoes a ferroelectric transition above the critical Ca concentration x_c=0. 0018, where doped Ca ions are substituted for the Sr ions [8–11] as shown in Fig. 1(b). The cubic structure above the structural phase-transition temperature T_{c1} changes in to the tetragonal structure below T_{c1} and into the rhombohedral structure below the ferroelectric transition temperature T_{c2}. The structural phase transition at T_{c1} is also antiferrodistortive as in pure $SrTiO_3$ at 105 K [8]. As in the case of impurity systems, Li-doped $KTaO_3$ and Nb-doped $KTaO_3$ [4], off-centered impurity ions are supposed. Their polarized dipole moments show a ferroelectric instability below the ferroelectric transition temperature [4]. In the case of Ca-doped$SrTiO_3$, a spontaneous polarization occurs along [110] directions in the *c* plane, where the tetragonal (D_{4h}) symmetry is lowered to C_{2v} [8]. With decreasing temperature a ferroelectric ordering process dominates, that is, due to the thermal growth of the polarization clouds surrounding the off-center Ca^{2+} dipoles [8]. The system behaves like a super paraelectric as the ferroelectric nano-ordered regions contain disordered cluster like regions. The investigation by x-ray and neutron diffractions and first-principles calculations [12] suggests that polar instabilities originating from the off-center displacements of

http://dx.doi.org/10.5772/45744

Ca^{2+} ions are not likely to directly polarize the host matrix by an electrostatic mechanism. Instead, the possible role of random fields in inducing the presence of disordered polar clusters was suggested, which is similar to polar nanoregions in relaxor materials.

Recently, a gigantic change in the dielectric constant by an ultraviolet (UV) illumination was discovered [13,14], and a deeper interest has been taken in $SrTiO_3$ again. The origin of the giant dielectric constants, however, has not yet been clarified. In Ca-doped $SrTiO_3$, it was reported that a UV illumination causes a ferroelectric peak shift of the dielectric constant toward the lower temperature side [11]. In several ferroelectric materials such as $BaTiO_3$ [15], SbSI [16], and oxygen-isotope-substituted $SrTiO_3$ [17], the T_c reduction under a UV illumination has been observed.

The optical information on the dielectric response is usually obtained from the experiments of Raman scattering or infrared spectroscopy. The usefulness of the investigation of low-frequency dielectric response by observing coherent phonons have also been demonstrated by the time-resolved study of the dynamics of phonons [18] and phonon polaritons [19]. At low frequencies this technique is very sensitive and provides a very good signal-to-noise ratio as compared to the conventional frequency-domain techniques while at higher frequencies a better performance will be achieved by using the conventional techniques. Therefore the coherent phonon spectroscopy and the conventional frequency-domain techniques can be considered to be complementary methods for the investigation of the dielectric response.

The observed signal of the Raman scattering [20] in $SrTiO_3$ is very weak because the distortion from cubic structure in the low-temperature phase is very small. The intensity of the first-order Raman signal is of the same order of magnitude with many second-order Raman signals, and then a background-free signal of the first-order Raman scattering cannot be observed.

Under a UV illumination, $SrTiO_3$ and Ca-doped $SrTiO_3$ show a broadband luminescence in the visible region originated from a relaxed excited state [21]. The coherent phonon spectroscopy is not sensitive to the luminescence and a powerful technique to investigate UV-illumination effects in paraelectric materials as compared to the Raman-scattering measurement because in Raman-scattering experiments, it is not easy to separate Raman-scattering signals from the luminescence.

In the present study, ultrafast polarization spectroscopy is used to observe the coherent optical phonons in pure and Ca-doped $SrTiO_3$, which are generated by femtosecond optical pulses through the process of impulsive stimulated Raman scattering [22,23]. Time-dependent linear birefringence induced by the generated coherent phonons is detected as a change of the polarization of probe pulses. High detection sensitivity of ~10^{-5} in polarization change has been achieved in our detection system. Damped oscillations of coherent phonons in $SrTiO_3$ were observed below the structural phase-transition temperature (T_c=105 K), and temperature dependences of the phonon frequency and the relaxation rate are measured [24]. The mechanism of the phonon relaxation is discussed by using a population decay model, in which an optical phonon decays into two acoustic phonons due to an harmonic phonon-phonon coupling.

The doping-induced ferroelectric phase transition in Ca-doped $SrTiO_3$ is investigated by observing the birefringence and coherent phonons [25]. In the birefringence measurement, the structural and the ferroelectric phase-transition temperatures are examined. In the observation of coherent phonons, the soft phonon modes related to the structural (T_{c1}=180 K) and the ferroelectric (T_{c2}=28 K) phase transitions are studied, and their frequencies are obtained from the observed coherent phonon signals. The behavior of the softening toward each phase-transition temperature and the UV-illumination effect on the ferroelectric transition are discussed. In addition to the ferroelectric phase transition at T_{c2}=28 K, another structural deformation at 25 K is found. A shift of the ferroelectric phase-transition temperature under the UV illumination and a decrease in the phonon frequencies after the UV illumination are found. We show the approach in the time domain is very useful for the study of the soft phonon modes and their UV-illumination effect in dielectric materials.

2. Experiment

The experiments are performed on single crystals of pure $SrTiO_3$ and Ca-doped $SrTiO_3$ with the Ca concentration of x=0.011. $SrTiO_3$ was obtained commercially (MTI Corporation) and Ca-doped $SrTiO_3$ was grown by the floating zone method [11]. The thickness of the sample is 1. 0 and 0.5 mm for the pure and Ca-doped crystals, respectively. In Ca-doped$SrTiO_3$, the structural phase-transition ($O_h \rightarrow D_{4h}$) temperature, T_{c1}=180 K, is obtained from the result of the birefringence measurement in section 3. The ferroelectric phase-transition temperature, T_{c2}=28 K, was determined by the measurement of dielectric constants [11]. The value of x was determined by the empirical relation of Bednorz and Müller [5].

Schematic diagram of the experiment of polarization spectroscopy is shown in Fig. 2. The change in optical anisotoropy (birefringence) is detected by a polarimeter as the change in the polarization of the probe light (ellipticity). In the birefringence measurement, the birefringence generated by the lattice deformation is detected by a continuous-wave (cw) probe beam with no pump beam. In the coherent phonon spectroscopy, the transient birefringence due to the coherent phonons generated by a pump pulse is detected by a probe pulse.

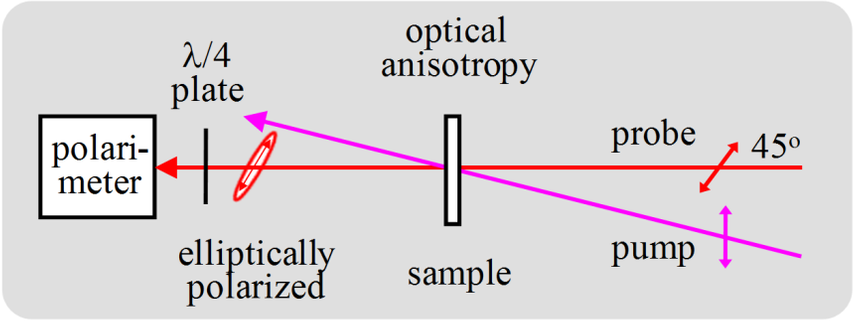

Figure 2. Schematic diagram of the experiment of polarization spectroscopy.

http://dx.doi.org/10.5772/45744

2.1. Birefringence measurement

In the birefringence measurement, the linearly polarized probe beam is provided by a Nd:YAG laser (532 nm, cw) and is perpendicular to the (001) surface of the sample.

The construction of the polarimeter is shown in Fig. 3. The polarimeter [26,27] detects the rotation of polarization plane of a light beam. A linearly-polarized beam is split by a polarized beam splitter (PBS) and incident on the two photodiodes (PD) whose photocurrents are subtracted at a resistor (R). When the polarized beam splitter is mounted at an angle of 45° to the plane of polarization of the light beam, the two photocurrents cancel. If the plane of polarization rotates, the two currents do not cancel and the voltage appears at the resistor.

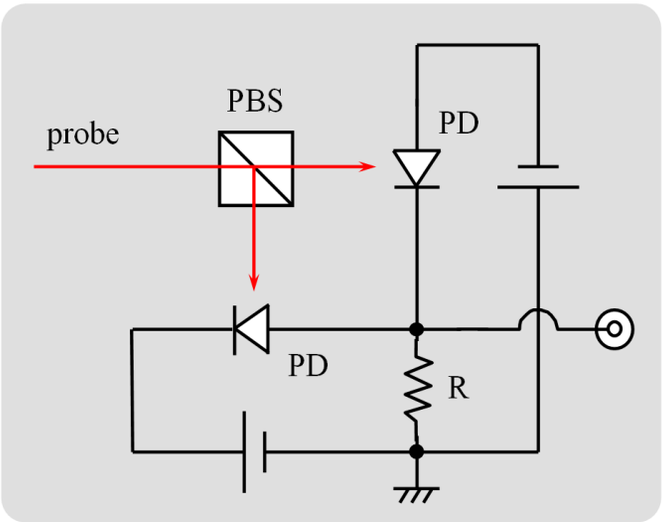

Figure 3. Construction of the polarimeter.

In the present experiment, the birefringence generated by the lattice deformation is detected as the change in polarization of the probe beam using a quarterwave plate and the polarimeter. The birefringence generated in the sample changes the linear polarization before transmission to an elliptical polarization after transmission. The linearly-polarized probe beam is considered to be a superposition of two circularly-polarized components which have the opposite polarizations and the same intensities. The generated birefringence destroys the intensity balance between the two components. The two circularly-polarized beams are transformed by the quaterwave plate to two linearly-polarized beams whose polarizations are crossed each other, and the unbalance of circular polarization is transformed to the unbalance of linear polarization or the rotation of polarization plane. This rotation is detected by the polarimeter as the signal of the lattice deformation.

2.2. Observation of coherent phonons

Coherent phonons are observed by ultrafast polarization spectroscopy with the pump-probe technique. The experimental setup for coherent phonon spectroscopy is shown in Fig. 4. Coherent phonons are generated by femtosecond optical pulses through the process of impulsive

stimulated Raman scattering [22,23], and are detected by monitoring the time-dependent anisotropy of refractive index induced by the pump pulse. The pump pulse is provided by a Ti: sapphire regenerative amplifier whose wavelength, pulse energy, and pulse width at the sample are 790 nm, 2 μJ, and 0.2 ps, respectively. The probe pulse is provided by an optical parametric amplifier whose wavelength, pulse energy, and pulse width are 690 nm, 0. 1 μJ, and 0.2 ps, respectively. The repetition rate of the pulses is 1kHz. The linearly polarized pump and probe beams are nearly collinear and perpendicular to the (001) surface of the sample, and are focused on the sample in a temperature-controlled refrigerator. The waist size of the beams at the sample is about 0.5 mm.

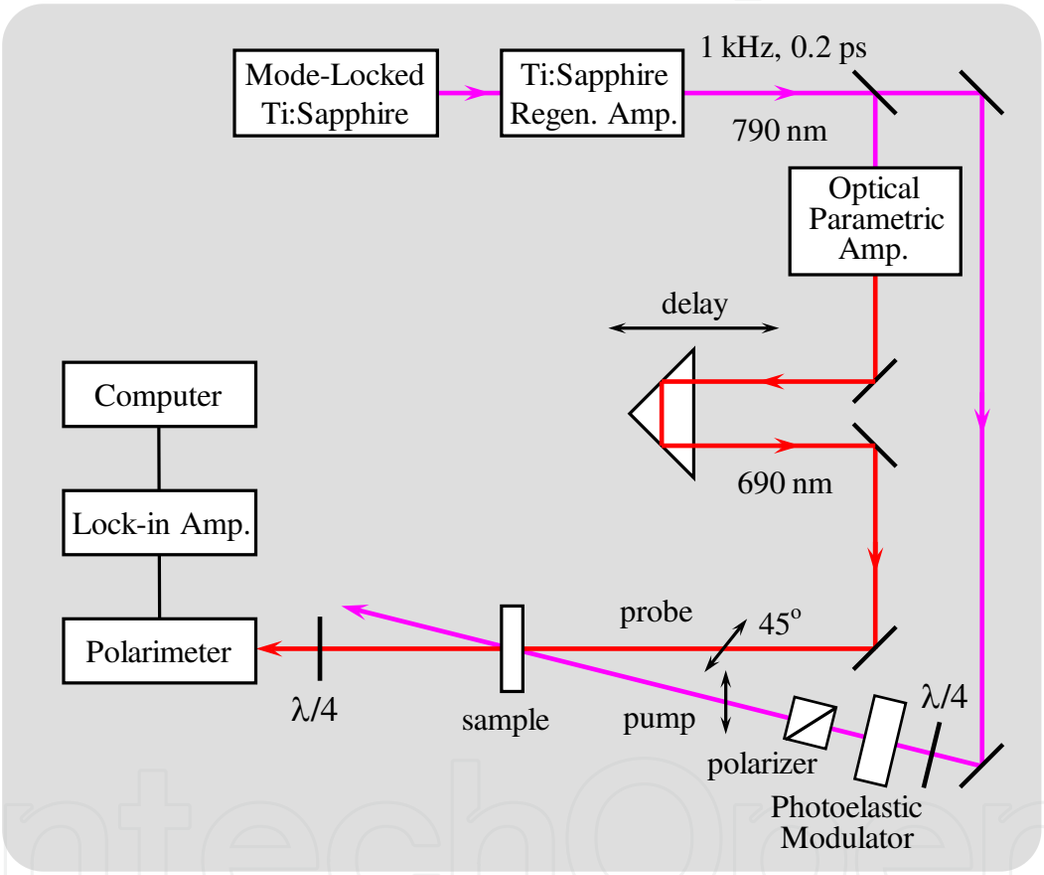

Figure 4. Experimental setup for coherent phonon spectroscopy.

The induced anisotropy of refractive index is detected by the polarimeter with a quarter-wave plate as the polarization change in the probe pulse. The plane of polarization of the probe pulse is tilted by 45° from that of the pump pulse. The two different wavelengths for the pump and probe pulses and pump-cut filters are used to eliminate the leak of the pump light from the input of the polarimeter. The time evolution of the signal is observed by changing the optical delay between the pump and probe pulses. The pump pulse is switched on and off shot by shot by using a photoelastic modulator, a quarter-wave plate, and a polarizer, and the output from the polarimeter is lock-in detected to improve the signal-to-noise ratio.

http://dx.doi.org/10.5772/45744

The source of UV illumination is provided by the second harmonics (380 nm, 3. 3 eV) of the output from another mode-locked Ti: sapphire laser, whose energy is larger than the optical band gap of $SrTiO_3$ (3.2 eV). Since the repetition rate of the UV pulses is 80 MHz, this UV illumination can be considered to be continuous in the present experiment, where the UV-illumination effect appearing more than one minute after is studied.

3. Birefringence measurement

Figure 5 shows the temperature dependences of the change in birefringence in $SrTiO_3$ and Ca-doped $SrTiO_3$ between 4.5 and 250 K, where the polarization plane of the probe light is along the [110]and [100]axes. In $SrTiO_3$, a change in birefringence appears below T_c=105 K, which is the temperature of the structural phase transition, and is increased as the temperature is decreased. In Ca-doped $SrTiO_3$, large changes in birefringence come out at T_{c1}=180 K, which is the temperature of the structural phase transition, and at T_{c2}=28 K, which is the temperature of the ferroelectric phase transition. The change in birefringence is increased as the temperature is decreased from T_{c1} to T_{c2}, as well as the case in $SrTiO_3$, and shows a increase in the gradient for both axes around T_{c2}. Below T_{c2}, another kind of lattice distortion is added, and the peaks of Δn due to the competition between the two kinds of lattice distortion appear. In both $SrTiO_3$ and Ca-doped$SrTiO_3$, a cusp on the birefringence curve appears around T_c=105 K and T_{c1}=180 K, respectively, because of the fluctuation associated with the second-order structural phase transition [28].

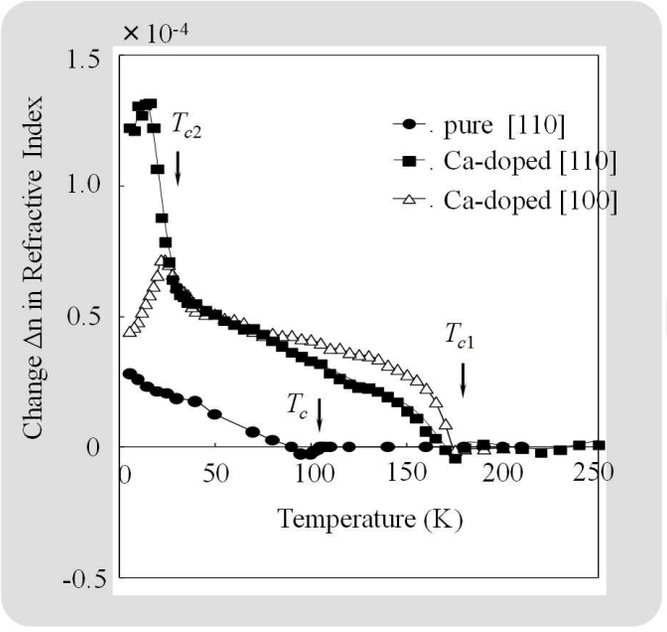

Figure 5. Temperature dependences of the change in birefringence between 4. 5 and 250 K in $SrTiO_3$ and Ca-doped $SrTiO_3$. The polarization plane of the probe light for $SrTiO_3$ is along the [110] axis (solid circles). That for Ca-doped $SrTiO_3$ is along the [110] axis (solid squares) and along the [100] axis (open triangles).

4. Coherent phonon spectroscopy in $SrTiO_3$

4.1. Angular dependence of the coherent phonon signal

Figure 6 shows the transient birefringence in $SrTiO_3$ observed at 6 K for the 0° pumping, where the polarization direction of the pump pulse is parallel to the [100] axis of the crystal. Vertical axis is the ellipticity η in electric-field amplitude of the transmitted probe pulse. At zero delay, a large signal due to the optical Kerr effect, whose width is determined by the pulse width, appears. After that, damped oscillations of coherent phonons are observed as shown in Fig. 6(b), where the vertical axis is enlarged by 50 from that of Fig. 6(a). The change of the polarization for the oscillation amplitude of the coherent phonon signal is 4×10^{-4} of the electric-field amplitudeof the probe pulse, which corresponds to the change $\Delta n=7\times10^{-8}$ of the refractive index. In our detection system, polarization change of ~10^{-5} in the electric field amplitude can be detected.

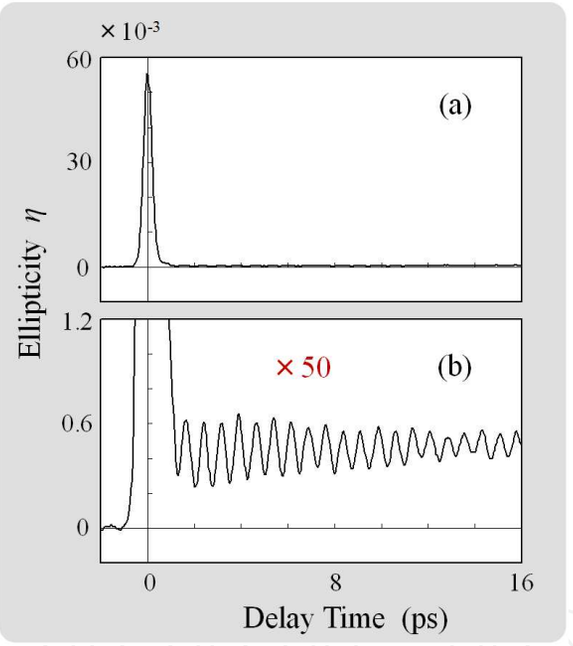

Figure 6. Transient birefringence in $SrTiO_3$ observed at 6 K for the 0° pumping. The vertical axis is the ellipticity η in electric-field amplitude of the transmitted probe pulse. (a) A large signal due to the optical Kerr effect appears at zero delay. (b) Damped oscillations of coherent phonons follow after the Kerr signal. The vertical axis of (b) is enlarged by 50 from that of (a).

Angular dependence of the coherent phonon signal in $SrTiO_3$ observed at 6 K is shown in Fig. 7(a), where the angle between the [100] axis of the crystal and the polarization direction of the pump pulse is 0°, 15°, and 45°. The angle between the polarization directions of the pump and probe pulses is fixed to 45°. The 0.7 ps period signal for the 0° pumping disappears for the 45°pumping, where the 2.3 ps period signal appears. The Fourier transform of the coherent phonon signals in Fig. 7(a) is shown in Fig. 7(b). Oscillation frequency of the signal for the 0° pumping is 1.35 THz, and that for the 45° pumping is 0.4 THz. For other

http://dx.doi.org/10.5772/45744

pumping angles both frequency components coexist in the coherent phonon signal. From the oscillation frequencies the 1.35 THz component is considered to correspond to the A_{1g} mode, and the 0.4 THz component to the E_g mode [7].

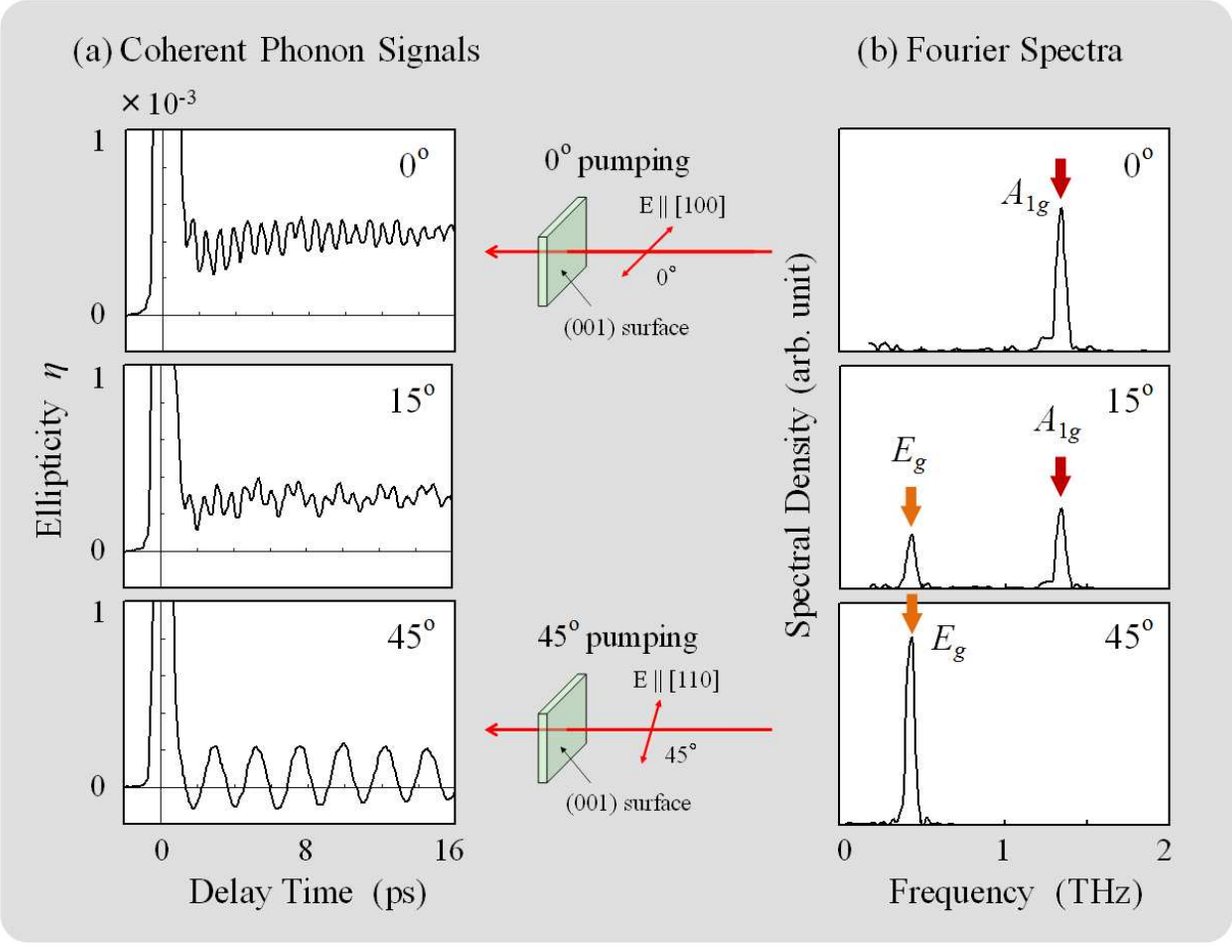

Figure 7. (a) Coherent phonon signals in $SrTiO_3$ observed at 6 K for the 0°, 15°, and 45° pumping, where the angle between the [100] axis of the crystal and the polarization direction of the pump pulse is changed. (b) Fourier transform of the coherent phonon signals in (a).

In addition to the oscillation signal there exists a dc component. The dc component has a maximum amplitude for the 0° pumping and minimum amplitude for the 45° pumping. However, the creation mechanism is not clear at present. In the following we pay attention to the oscillation component.

4.2. Temperature dependence of the coherent phonon signal

The temperature dependence of the coherent phonon signal in $SrTiO_3$ observed for the 0° pumping, which corresponds to the A_{1g} mode, is shown in Fig. 8(a). The oscillation period and the relaxation time of coherent phonons at 10 K are 0.7 and 12 ps. As the temperature is increased, the oscillation period becomes longer and the relaxation time becomes shorter. At

T_c=105 K, the phase transition point, the oscillation disappears. Above T_c no signal of coherent phonons is observed. The temperature dependence of the coherent phonon signal in $SrTiO_3$observed for the 45° pumping, which corresponds to the E_g mode, is shown in Fig. 8(b). The oscillation period and the relaxation time of coherent phonons at 10 K are 2.3 and 45 ps. Similar behavior to that of the A_{1g} mode was observed as the temperature was increased.

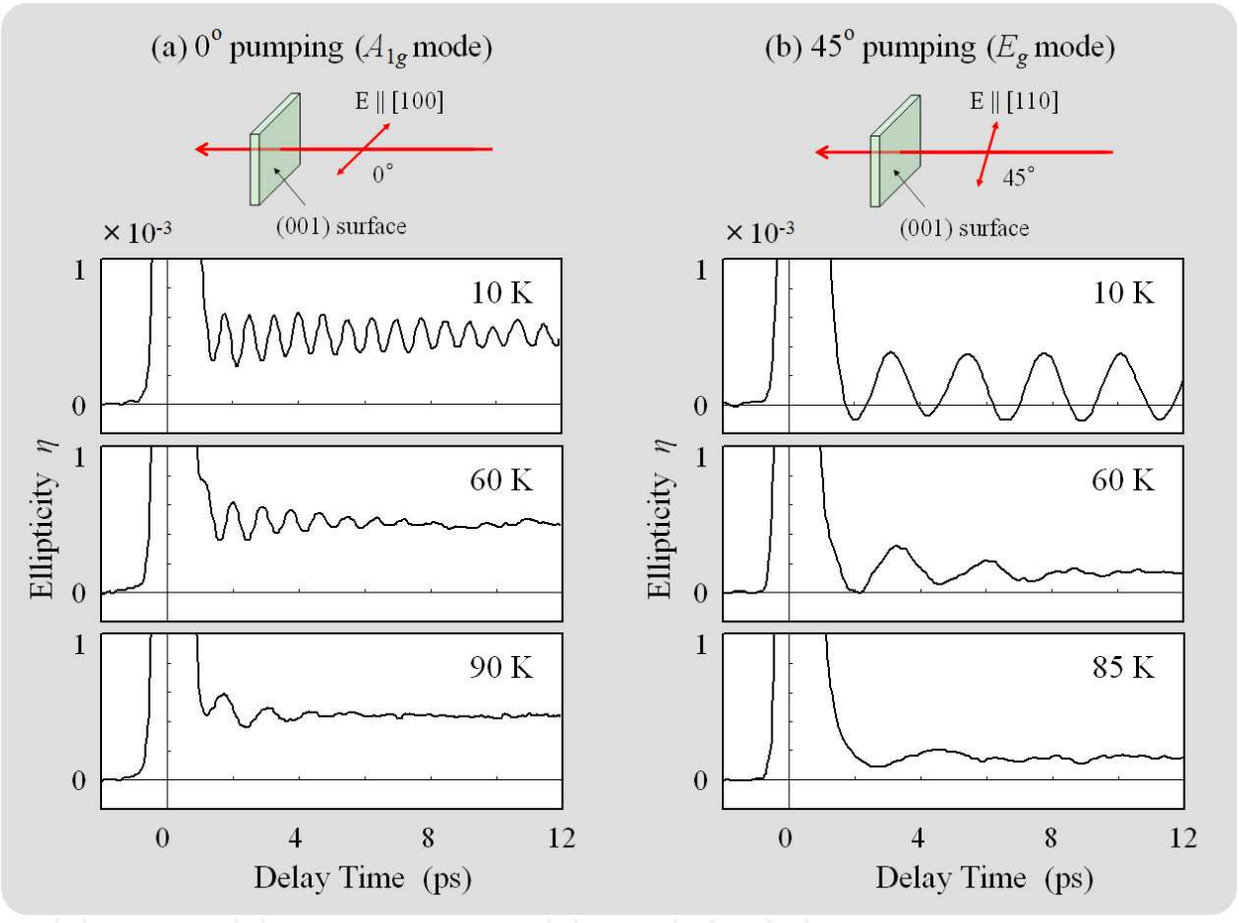

Figure 8. Temperature dependence of the coherent phonon signals in $SrTiO_3$ observed (a) for the 0° pumping which corresponds to the A_{1g} mode and (b) for the 45° pumping which corresponds to the E_g mode.

4.3. Phonon frequencies

The observed coherent phonon signal $S(t)$ is expressed well by the damped oscillation

$$S(t) = Ae^{-\gamma t}\sin \omega t \ , \tag{1}$$

where ω is the oscillation frequency and γ is the relaxation rate. This sine-type function is expected for phonons induced by impulsive stimulated Raman scattering [22,23]. The temperature dependence of the oscillation frequency in $SrTiO_3$ obtained from the observed co-

http://dx.doi.org/10.5772/45744

herent phonon signal below T_c is shown in Fig. 9. The diamonds are the oscillation frequency for the A_{1g} mode, and the squares are that for the E_g mode. As the temperature is increased from 6 K, the oscillation frequencies decrease and approach zero at the phase transition temperature T_c for both modes. This result is consistent with the temperature dependence of phonon frequency observed by Raman scattering [7]. The solid curves describe a temperature dependence of the form $\omega \propto (T_c - T)^n$. The experimental results for the temperature region between 50 K and T_c are explained well by n=0.4 for both modes, while those below 40 K deviate from that form.

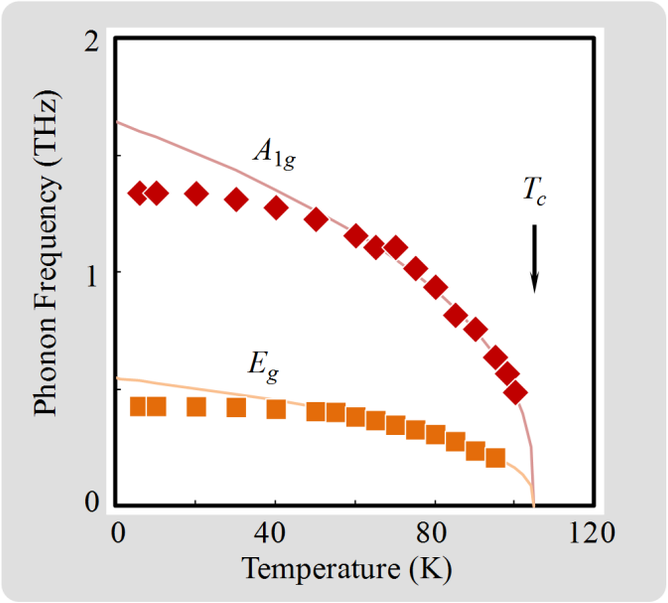

Figure 9. Temperature dependence of the oscillation frequency in $SrTiO_3$ obtained from the coherent phonon signal below T_c. The diamonds are the oscillation frequency for the A_{1g} mode, and the squares are that for the E_g mode. The solid curves describe a temperature dependence of the form $\omega \propto (T_c - T)^n$, where T_c=105 K and n=0.4 for both modes.

The intensity of the first-order Raman-scattering signal in $SrTiO_3$ is very weak and is of the same order of magnitude as many second-order Raman-scattering signals because the distortion from the cubic structure in the low-temperature phase is very small. Then observation of a background-free signal of first-order Raman scattering is not easy, and information on the relaxation, or the spectral width, is not given in a study of Raman scattering [20]. By the present method of coherent phonon spectroscopy in the time domain, on the other hand, background-free damped oscillations can be observed directly, and the oscillation frequency and the relaxation rate can be obtained accurately.

4.4. Relaxation rates

The temperature dependence of the relaxation rate in $SrTiO_3$ obtained from the observed coherent phonon signal below T_c is shown in Fig. 10. The diamonds in Fig. 10(a) are the relaxation rate for the A_{1g} mode and the squares in Fig. 10(b) are that for the E_g mode. The relaxation rates increase as the temperature is increased.

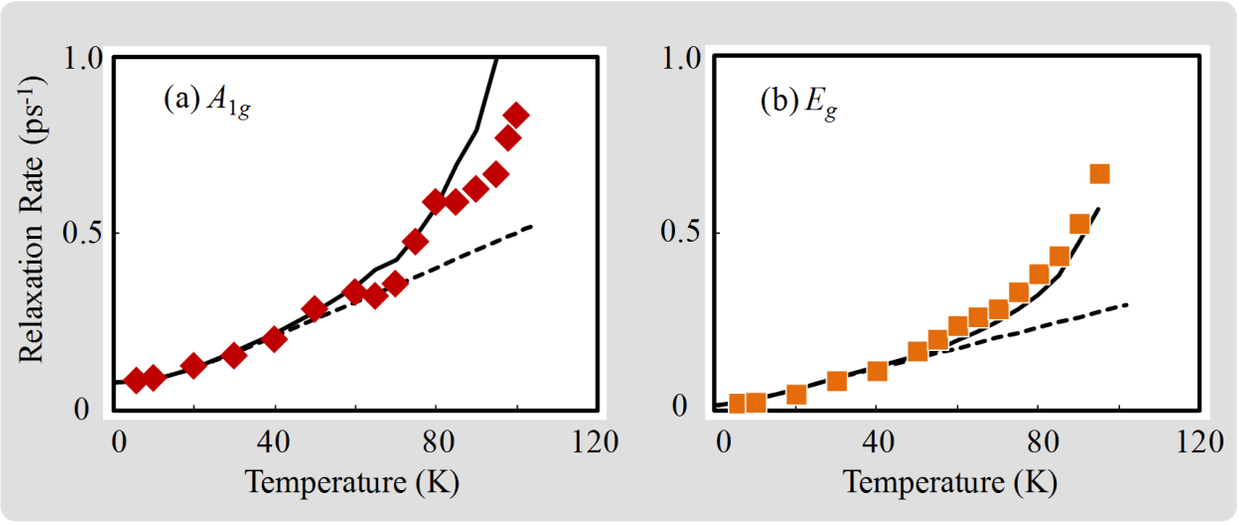

Figure 10. Temperature dependence of the relaxation rate in $SrTiO_3$ obtained from the coherent phonon signal below T_c. (a) The diamonds are the relaxation rate for the A_{1g} mode, and (b) the squares are that for the E_g mode. The solid curves show the theoretical curves including the frequency change obtained from Eq. (2).

In general, relaxation of coherent phonons is determined by population decay (inelastic scattering) and pure dephasing (elastic scattering). In metals, pure dephasing due to electron-phonon scattering, which depends on the hot electron density, contributes to the phonon relaxation [29]. In dielectric crystals, the relaxation process of the coherent phononis considered to be dominated by the population decay due to the anharmonic phonon-phonon coupling [30-32], rather than pure dephasing. According to the anharmonic decay model [30], the relaxation of optical phonons in the center of the Brillouin zone is considered to occur through two types of decay process, the down-conversion and up-conversion processes. In a down-conversion process, the initial ω_0 phonon with wave vector $k \cong 0$ decays into two lower-energy phonons ω_i and ω_j, with opposite wave vectors k and $-k$, which belong to the i branch and the j branch of the phonon. Energy and wave-vector conservation is given by $\omega_0=\omega_{ik}+\omega_{j-k}$. In an up-conversion process, the initial excitation is scattered by a thermal phonon (ω_{ik}) into a phonon of higher energy (ω_{jk}), where $\omega_0+\omega_{ik}=\omega_{jk}$. The down-conversion process can be realized either for $i= j$ (overtone channel), or for $i\neq j$ (combination channel), depending on the phonon band structure of the material, while the up-conversion process contains only the combination channel and has no overtone channel. The combination channel is less likely, because three frequencies of phonons and three phonon branches have to be concerned and stringent limitations are imposed by the energy and wave-vector conservation. The overtone channel, on the other hand, is more likely because two (an optical and an acoustic) phonon branches are concerned, and the energy and wave-vector conservation are necessarily satisfied by two acoustic phonons with the same frequency and opposite wave vectors, if the frequency maximum of the acoustic branch is higher than half the frequency of the initial optical phonon.

Here we consider the down-conversion process in which an optical phonon decays into two acoustic phonons with half the frequency of the optical phonon and with opposite wave vec-

http://dx.doi.org/10.5772/45744

tors. Schematic diagram of this down-conversion process is shown in Fig. 11. The temperature dependence of the relaxation rate γ of the coherent phonon is given by [30,31]

$$\gamma = \gamma_0 \left(1 + \frac{2}{\exp\left[\hbar(\omega_0 / 2) / k_B T \right] - 1} \right) \tag{2}$$

where ω_0 is the frequency of the optical phonon, and k_B is the Boltzmann constant.

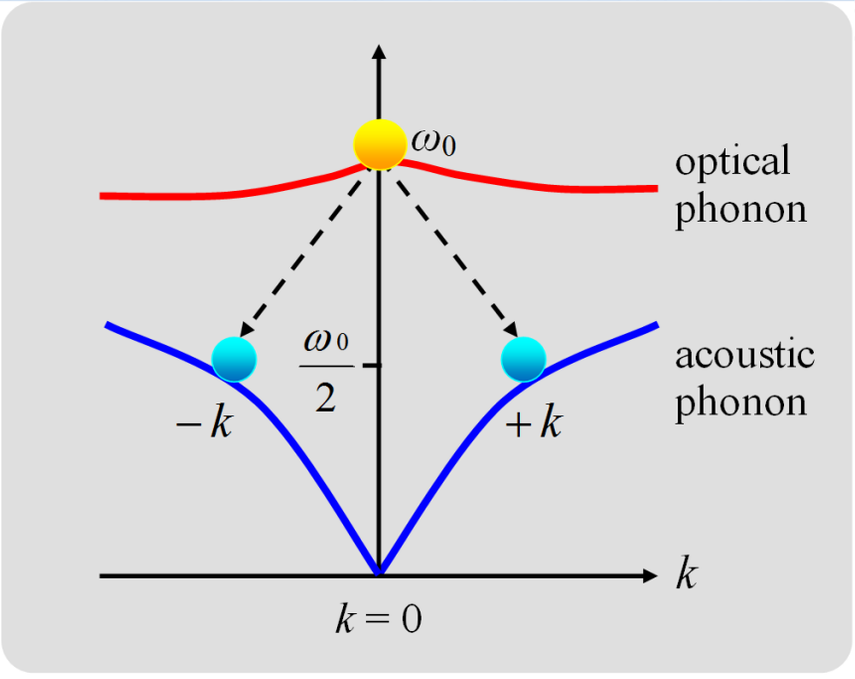

Figure 11. Schematic diagram of the down-conversion processe (overtone channel) in the an harmonic decay model of optical phonons. The initial ω_0 optical phonon with wave vector $k \cong 0$ decays into two $\omega_0 / 2$ acoustic phonons, with opposite wave vectors k and $-k$.

In ordinary materials the temperature dependence of the phonon frequency is small, and a theoretical curve with a fixed value of phonon frequency fits the experimental data well. In $SrTiO_3$, however, the phonon frequencies are changed greatly as the temperature is increased; thus a frequency change has to be considered. The solid curves in Fig. 10 show the theoretical curves including the frequency change obtained from Eq. (2) with γ_0=8. 0×10^{10} s^{-1} for the A_{1g} mode and 1.5×10^{10} s^{-1} for the E_g mode, where the observed phonon frequencies in Fig. 9 are used for each temperature. The broken curves show the theoretical curves in the case of no frequency change. As is seen in Fig. 10, the solid curves explain well the experimental data.

Deviation of the experimental data near T_c from the solid curve may be caused by the effect of the phase transition. However, the relaxation rate just around the phase transition point cannot be obtained in the present experiment, and the relation between the temperature-dependent relaxation rate and the structural phase transition is not clear.

5. Coherent phonon spectroscopy in Ca-doped $SrTiO_3$

5.1. Angular dependence of the coherent phonon signal

The angular dependence of the coherent phonon signal in Ca-doped $SrTiO_3$ observed at 50 K is shown in Fig. 12(a), where the angle between the [100] axis of the crystal and the polarization plane of the pump pulse is 0°, 25°, and 45°. The angle between the polarization planes of the pump and probe pulses is fixed to 45°. Vertical axis is the ellipticity in electric field amplitude of the transmitted probe. At zero delay, a large signal due to the optical Kerr effect, whose width is determined by the laser-pulse width, appears. After that, damped oscillations of coherent phonons are observed. For the 0° pumping a 0.5 ps period signal appears while it disappears for the 45° pumping and a 2 ps period signal appears. TheFourier transform of the coherent phonon signals in Fig. 12(a) is shown in Fig. 12(b). The oscillation frequency of the signalfor the 0° pumping is 1.9 THz and that for the 45° pumping is 0.5 THz. For other pumping angles both frequency components coexist in the coherent phonon signal. These phonon modes are the soft modes related to the structural phase transition at T_{c1}=180 K. From the oscillation frequencies the 1.9 THz component corresponds to the A_{1g} mode, and the 0.5 THz components to the E_g mode, which are assigned from the modes of pure $SrTiO_3$ [7] and from that of $Sr_{1-x}Ca_xTiO_3$ (x=0.007) [8].

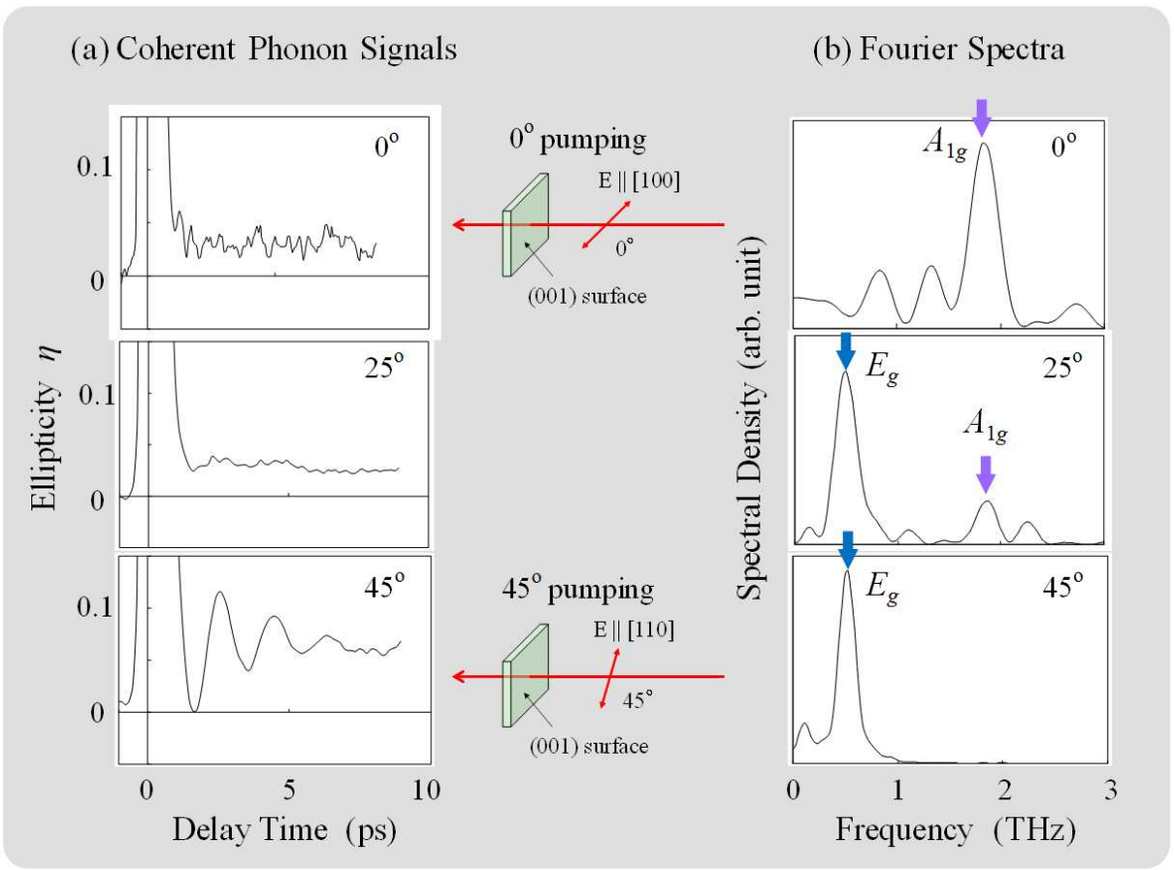

Figure 12. (a) Coherent phonon signals in Ca-doped $SrTiO_3$ observed at 50 K for the 0°, 25°, and 45° pumping, where the angle between the [100] axis of the crystal and the polarization direction of the pump pulse is changed. (b) Fourier transform of the coherent phonon signals in (a).

http://dx.doi.org/10.5772/45744

5.2. Temperature dependence of the coherent phonon signal

The temperature dependence of the coherent phonon signal in Ca-doped $SrTiO_3$ observed for the 45° pumping, which corresponds to the E_g mode, is shown in Fig. 13. At 6 K some oscillation components, which have different frequencies, are superposed. As the temperature is increased, the number of the oscillation components is decreased, the oscillation period becomes longer and the relaxation time becomes shorter. At T_{c1}=180 K, which is the structural phase-transition temperature obtained from the birefringence measurement, no signal of coherent phonons is observed.

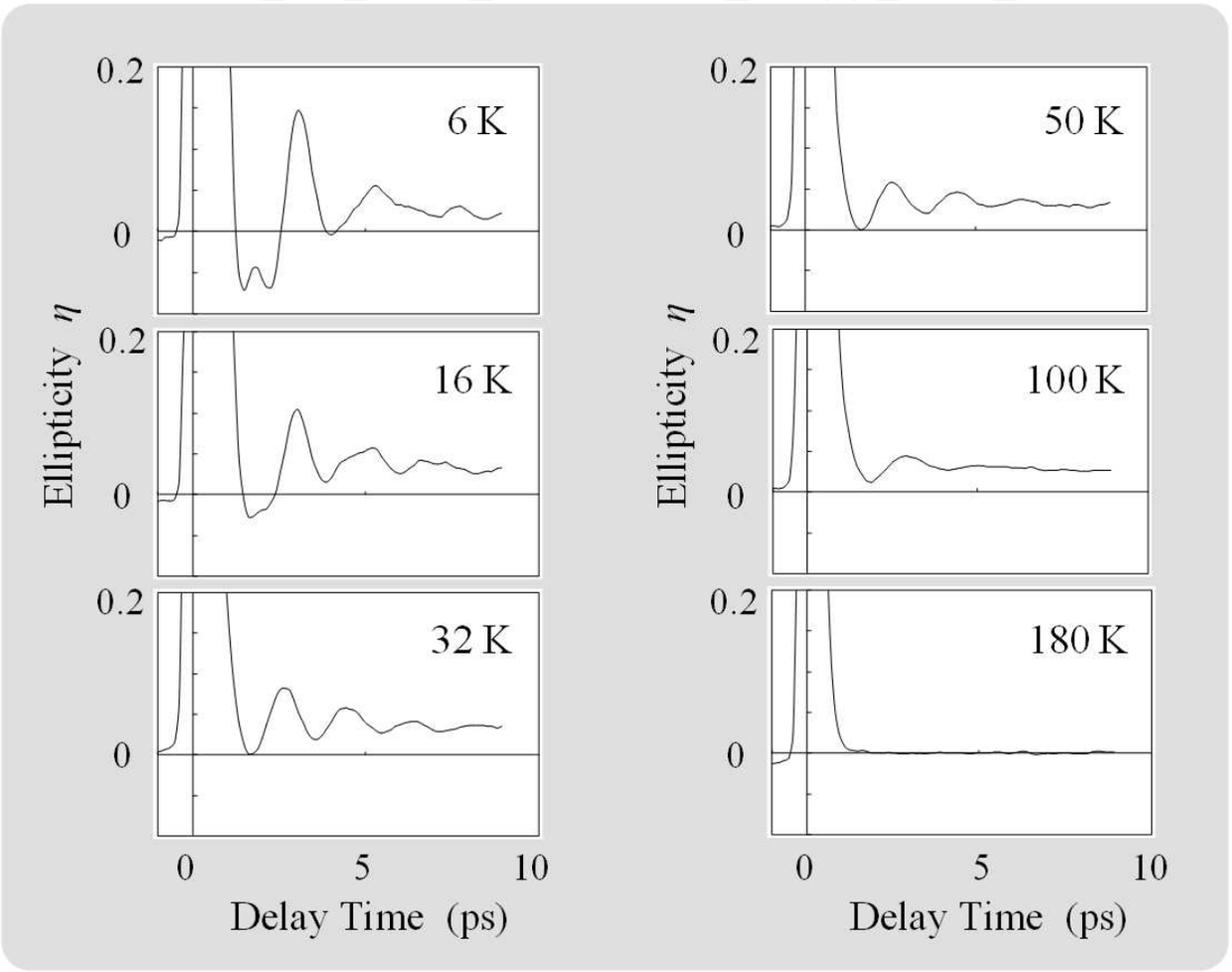

Figure 13. Temperature dependence of the coherent phonon signal in Ca-doped SrTiO3 observed for the 45° pumping.

The temperature dependence of the coherent phonon signal in Ca-doped $SrTiO_3$ observed for the 25° pumping are shown in Figs. 14 and 15. Figure 14(a) shows the coherent phonon signals below the ferroelectric phase-transition temperature T_{c2} and Fig. 15(a) shows those above T_{c2}. Figure 14(b) shows the Fourier transform of the coherent phonon signals in Fig. 14(a), where the peaks with arrows 1, 2, and 3 correspond to the ferroelectric phonon modes [8]. Figure 15(b) shows the Fourier transform of the coherent phonon signals in Fig. 15(a), where modes 1, 2, and 3 disappear but the A_{1g} and E_g modes related to the structural phase-transition remain.

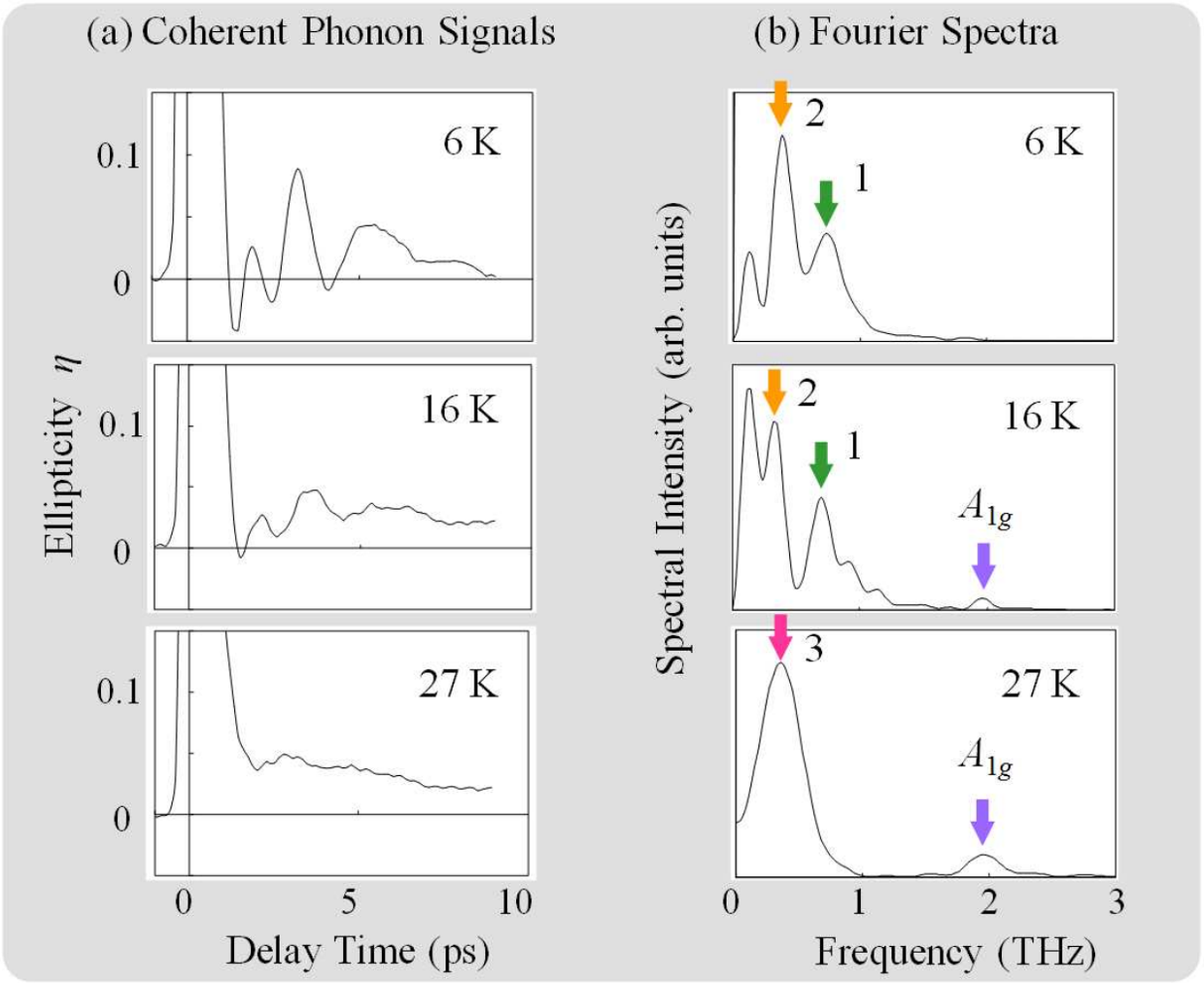

Figure 14. (a) Temperature dependence of the coherent phonon signal in Ca-doped $SrTiO_3$ observed for the 25° pumping below the ferroelectric phase-transition temperature T_{c2}. (b) Fourier transform of the coherent phonon signals in (a).

5.3. Phonon frequencies

Each component of the coherent phonon signal is expressed well by damped oscillations in Eq. (1). The temperature dependence of the oscillation frequencies in Ca-doped $SrTiO_3$ obtained from the observed coherent phonon signals below T_{c1} is shown in Fig. 16. The solid circles are the oscillation frequencies for the A_{1g} and E_g modes. The triangles are that for modes 1, 2, and 3 which are related to the ferroelectric phase transition. As for the A_{1g} and E_g modes, as the temperature is increased from 6 K, the oscillation frequencies decrease and approach to zero at the structural phase-transition temperature T_{c1} for both modes. This result is consistent with the temperature dependence of phonon frequency observed by Raman scattering [7] and coherent phonons in section 4.3 for pure $SrTiO_3$ except for the phase-transition temperature. The broken curves describe a temperature dependence of the form $\omega \propto (T_c - T)^n$. The experimental results for the temperature region between T_{c1} and T_{c2} are explained well by n=0.5 for both modes. Below the ferroelectric phase-transition temperature T_{c2}, another mode appears at 0.9 THz. It is

http://dx.doi.org/10.5772/45744

considered that the doubly degenerate E_g mode is split into two components under the tetragonal-to-rhombohedrallattice distortion.

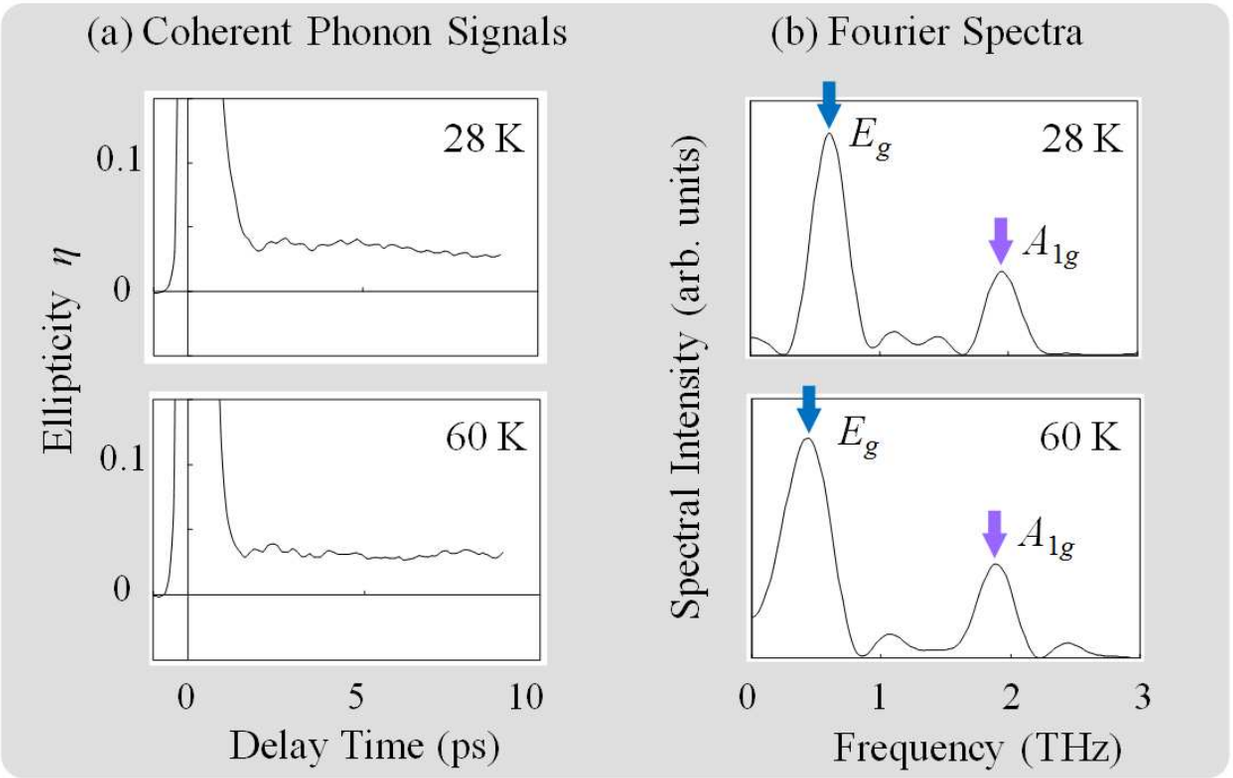

Figure 15. (a) Temperature dependence of the coherent phonon signal in Ca-doped $SrTiO_3$ observed for the 25° pumping above the ferroelectric phase-transition temperature T_{c2}. (b) Fourier transform of the coherent phonon signals in (a).

The temperature dependence of the phonon frequencies, which are related to the ferroelectric phase transition, obtained from the observed coherent phonon signals below T_{c2} is shown in Fig. 17, where only the frequencies of the reproducible peaks in the Fourier spectrum are plotted. While the lowest peaks at 6 and 16 K in Fig. 14, for example, may be the third mode observed in the Raman experiment [8], the frequencies of the peaks with poor reproducibility are not plotted in Figs. 16 and 17. Under dark illumination, two phonon modes 1 and 2 are softened toward about 25 K and degenerate into mode 3, which seems to be softened toward the ferroelectric phase-transition temperature T_{c2}=28 K. The lift of degeneracy for mode 3 below T_{c2} suggests that another structural deformation occurs at 25 K. In the Raman-scattering experiment [8], three modes deriving from the TO_1 mode has been observed. The three modes do not all split off at the same temperature; the highest-energy component splits off at the ferroelectric transition temperature while the other two split off at the temperature about 3 K lower. These two temperatures may correspond to the two temperatures, 28 and 25 K, observed in our experiment, and the temperature differences are nearly equal to each other. The existence of the second structural deformation at 25 K is consistent with the Raman-scattering data.

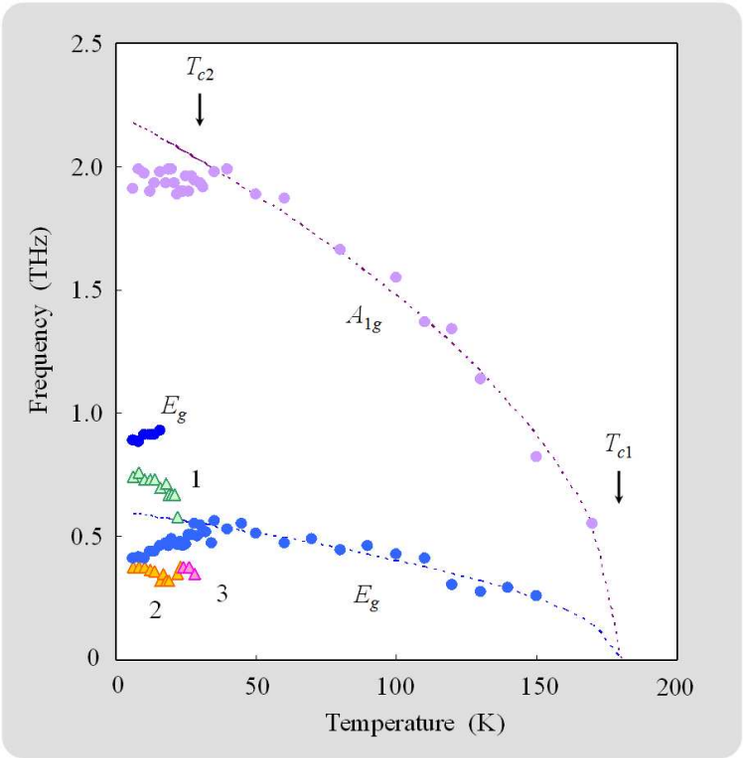

Figure 16. Temperature dependence of the phonon frequencies in Ca-doped SrTiO3 obtained from the coherent phonon signals below T_{c1}. The solid circles are the oscillation frequencies for the A_{1g} and E_g modes. The broken curves describe a temperature dependence of the form $\omega \propto (T_c - T)^n$, where T_c=180 K and n=0.5 for both modes. The triangles are that for modes 1, 2, and 3 related to the ferroelectric phase transition.

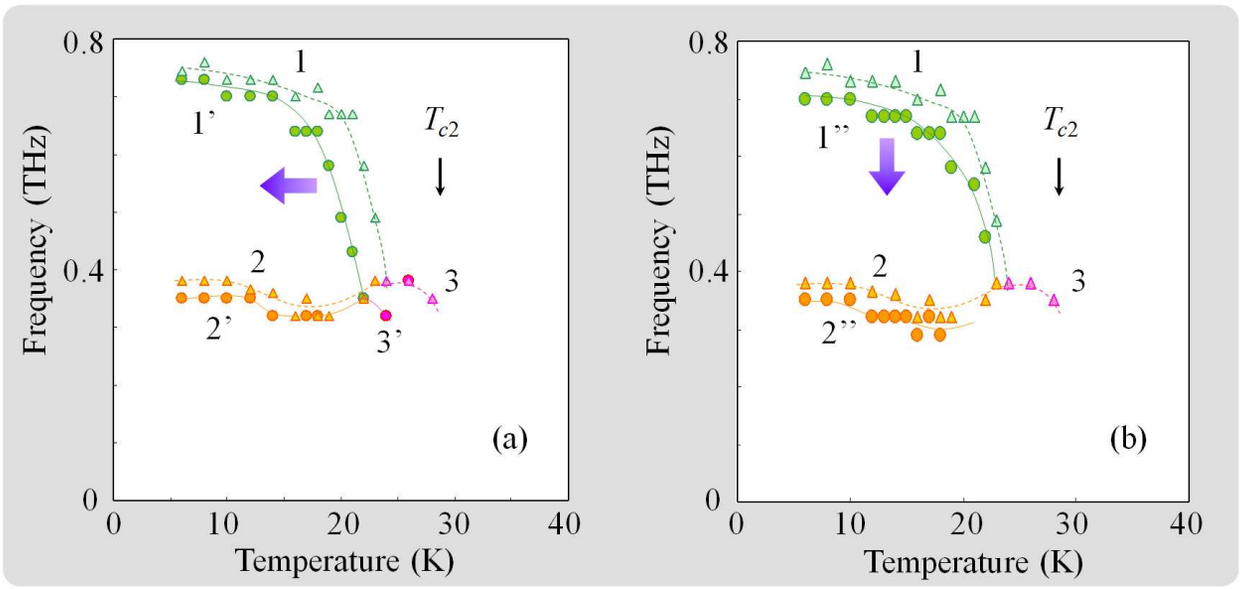

Figure 17. Temperature dependence of the phonon frequencies (a) under dark (1, 2, 3) and under UV (1′,2′,3′) illumination below T_{c2}, which correspond the phonon modes related to the ferroelectric phase transition, and (b)under dark (1, 2, 3) and after UV(1′′,2′′,3′′) illumination, where the intensity of the UV illumination is 7 mW/mm^2.

http://dx.doi.org/10.5772/45744

5.4. UV-illumination effect

In order to examine the UV-illumination effect, two types of measurements, under the UV illumination and after the UV illumination, are carried out. The temperature dependence of the phonon frequencies under the UV illumination is shown in Fig. 17(a), where the intensity of the UV illumination is 7 mW/mm^2. As is seen in Fig. 17(a), the temperature, toward which the two modes 1 and 2 are softened and degenerate into mode 3, shifts to the lower temperature side. The temperature shift due to the UV-illumination effect is ~3 K.

Doped Ca ions behave as permanent dipoles and ferroelectric clusters are formed around Ca dipoles with high polarizability of the host crystal. The ferroelectric transition is caused by the ordering of randomly distributed Ca dipoles. The UV-illumination-induced T_{c2} reduction is related to the screening of the internal macroscopic field by UV-excited carriers. Under the UV-illumination non equilibrium carriers appear, which are captured by traps and screen the polarization field. The ordering is prevented by the photo excited carriers. Thus, the screening effect due to the UV-excited carriers weakens the Coulomb interaction between dipoles, and the transition temperature is decreased.

The theoretical T_{c2} reduction under the UV illumination ΔT_{c2} is given by [11]

$$\frac{\Delta T_{c2}}{T_{c2}(0)} = 1 - \left(1 + \lambda a + \frac{\gamma}{4\pi}\lambda^2 a^2\right)\exp(-\lambda a), \tag{3}$$

where $T_{c2}(0)$ is the transition temperature before the UV illumination, λ is the inverse of the screening length, a is the mean separation between the dipoles, and γ is the number of the nearest-neighbor dipoles. The expression of λ is presented by $\lambda = \sqrt{ne^2 / \varepsilon\varepsilon_0 k_B T}$, where n is the carrier concentration which depends on the UV-illumination intensity and ε is the relative dielectric constant. In the present case, the domain is large enough and the dipole-dipole interaction is expressed as a simple Coulomb interaction. The UV-illumination-intensity dependence of the T_{c2} reduction for $Sr_{1-x}Ca_xTiO_3$ (x=0. 011) was analyzed by using Eq. (3). Assuming that the carrier concentration is proportional to the UV-illumination intensity, the fitting result reproduced well the experimental result obtained in the measurement of dielectric constants [11]. Here we estimate the inverse λ of the screening length at the UV-illumination intensity of 7 mW/mm^2. As a result of the measurement of dielectric constant [11], the carrier concentration is n=2. 5× 10^{17} cm^{-3} at 3 mW/mm^2. From this value we can estimate the carrier concentration to be n=5. 8× 10^{17} cm^{-3} at 7 mW/mm^2. The value of the inverse of the screening length is obtained as

$$\lambda = \sqrt{\frac{ne^2}{\varepsilon\varepsilon_0 k_B T}} = \sqrt{\frac{8\pi n a_B E_{1s}}{\varepsilon k_B T}} = 1.1 \times 10^7 \text{ cm}^{-1}, \tag{4}$$

where a_B and E_{1s} are Bohr radius and the energy of the hydrogen atom in the 1s ground state, respectively, and we use the dielectric constant ε=4 in the visible region. Substituting the value of λ into Eq. (3), the shift of the transition temperature can be estimated to be ΔT_{c2}~8 K. This estimation is not inconsistent with the observed values of the temperature shift in the

experiment of coherent phonons, in which the value of the observed transition temperature shift is ~3 K.

The temperature dependence of the phonon frequencies after the UV illumination is shown in Fig. 17(b), where theUV illumination of 7 mW/mm^2 is on before the coherent phonon measurement but is off during the measurement. In this case, on the other hand, the shift of the softening temperature for modes 1 and 2 is not clear. The phonon frequencies for modes 1 and 2 are decreased while the coherent phonon signal for mode 3 is not observed. The relaxation time of the UV-illumination induced carriers is on the order of milliseconds below 30 K for $SrTiO_3$ [21]. As is seen in Fig. 17(b), however, it is suggested that the UV-illumination effect, frequency decrease for modes 1 and 2 and disappearance of mode-3 signal, remains for at least several minutes, even if the UV illumination is switched off, although the T_{c2} shifting effect disappears immediately.

6. Summary

We observed coherent phonons in pure and Ca-doped $SrTiO_3$ using ultrafast polarization spectroscopy to study the ultrafast dynamics of soft phonon modes and their UV-illumination effect. Coherent phonons are generated by linearly polarized pump pulses. The time-dependent linear birefringence induced by the generated coherent phonons is detected asa change of the polarization of the probe pulses. A high detection sensitivity of ~10^{-5} in polarization change, which corresponds to the change Δn=2× 10^{-9} of the refractive index for a 1 mm sample, has been achieved in our detection system.

In $SrTiO_3$, damped oscillations of coherent phonons for the A_{1g} and E_g modes, which contribute to the structural phase transition at 105 K, were observed. The temperature dependences of the frequency and the relaxation rate of the observed coherent phonons were measured. Softening of the phonon frequencies was observed. The phonon relaxation is explained well by a decay model of a frequency-changing phonon, in which the optical phonon decays into two acoustic phonons due to the anharmonic phonon-phonon coupling.

We observed the temperature dependences of the birefringence and the coherent phonon signal to investigate the doping-induced ferroelectric phase transition in Ca-doped$SrTiO_3$ with the Ca concentration of x=0.011. In the birefringence measurement, it was confirmed that the structural phase-transition temperature is T_{c1}=180 K. Coherent phonons were observed by using ultrafast polarization spectroscopy. The damped oscillations of coherent phonons for the A_{1g} and E_g modes, which contribute to the structural phase transition at T_{c1}=180 K, and for the modes 1, 2, and3, which contribute to the ferroelectric phase transition at T_{c2}=28 K, were observed. The phonon frequencies were obtained from the observed signals of coherent phonons, and their softening toward each phase-transition temperature was observed. Another structural deformation at 25 K was found in addition to the ferroelectric phase transition at T_{c2}. It was found that the UV illumination causes the shift of the ferroelectric phase-transition temperature toward the lower temperature side, and the temperature

http://dx.doi.org/10.5772/45744

shift is ~3 K. The decrease in the phonon frequencies after the UV illumination suggests the UV-illumination effect remains even if the UV illumination is switched off.

It was shown that the coherent phonon spectroscopy in the time domain is a very useful approach to study the soft phonon modes and their UV-illumination effect in dielectric materials.

Acknowledgement

We would like to thank Dr. Y. Koyama for experimental help and Dr. Y. Yamada and Prof. K. Tanaka for providing us the samples of Ca-doped $SrTiO_3$.

Author details

Toshiro Kohmoto

Graduate School of Science, Kobe University, Japan

References

[1] K. A. Müller and H. Burkard, Phys. Rev. B 19, 3593 (1979).

[2] H. Uwe and T. Sakudo, Phys. Rev. B 13, 271 (1976).

[3] M. Itoh, R. Wang, Y. Inaguma, T. Yamaguchi, Y.-J. Shan, and T.Nakamura, Phys. Rev. Lett. 82, 3540 (1999).

[4] B. E. Vugmeister and M. P. Glinchuk, Rev. Mod. Phys. 62, 993 (1990).

[5] J. G. Bednorz and K. A. Müller, Phys. Rev. Lett. 52, 2289 (1984).

[6] J. F. Scott, Rev. Mod. Phys. 46, 83 (1974), and references therein.

[7] P. A. Fleury, J. F. Scott, and J. M. Worlock, Phys. Rev. Lett. 21,16 (1968).

[8] U. Bianchi, W. Kleemann, and J. G. Bednorz, J. Phys.: Condens. Matter 6, 1229 (1994).

[9] U. Bianchi, J. Dec, W. Kleemann, and J. G. Bednorz, Phys. Rev. B 51, 8737 (1995).

[10] Bürgel, W. Kleemann, and U. Bianchi, Phys. Rev. B 53, 5222 (1995).

[11] Y. Yamada and K. Tanaka, J. Phys. Soc. Jpn. 77, 5 (2008).

[12] G. Geneste and J.-M. Kiat, Phys. Rev. B 77, 174101 (2008).

[13] M. Takesada, T. Yagi, M. Itoh, and S. Koshihara, J. Phys. Soc. Jpn. 72, 37 (2003).

[14] T. Hasegawa, S. Mouri, Y. Yamada, and K. Tanaka, J. Phys. Soc. Jpn. 72, 41 (2003).

[15] G. Godefroy, P. Jullien, and L. Cai, Ferroelectrics 13, 309 (1976).

[16] S. Ueda, I. Tatsuzaki, and Y. Shindo, Phys. Rev. Lett. 18, 453 (1967).

[17] Y. Yamada and K. Tanaka, J. Lumin. 112, 259 (2005).

[18] T. P. Dougherty, G. P. Wiederrecht, K. A. Nelson, M. H. Garrett,H. P. Jensen, and C. Warde, Science 258, 770 (1992).

[19] H. J. Bakker, S. Hunsche, and H. Kurz, Rev. Mod. Phys. 70, 523 (1998).

[20] W. G. Nilsen and J. G. Skinner, J. Chem. Phys. 48, 2240 (1968).

[21] T. Hasegawa, M. Shirai, and K. Tanaka, J. Lumin. 87-89, 1217 (2000).

[22] Y.-X. Yan, E. B. Gamble, Jr., and K. A. Nelson, J. Chem. Phys.83, 5391 (1985).

[23] G. A. Garrett, T. F. Albrecht, J. F. Whitaker, and R. Merlin, Phys. Rev. Lett. 77, 3661 (1996).

[24] T. Kohmoto, K. Tada, T. Moriyasu, and Y. Fukuda,Phys. Rev. B 74, 064303 (2006).

[25] Y. Koyama, T. Moriyasu, H. Okamura, Y. Yamada, K. Tanaka, and T. Kohmoto, Phys. Rev. B 81, 024104 (2010).

[26] T. Kohmoto, Y. Fukuda, M. Kunitomo, and K. Isoda, Phys. Rev. B 62, 579 (2000).

[27] R. V. Jones, Proc. R. Soc. London, Ser. A 349, 423 (1976).

[28] E. Courtens, Phys. Rev. Lett. 29, 1380 (1972).

[29] K. Watanabe, N. Takagi, and Y. Matsumoto, Phys. Rev. Lett. 92,057401 (2004).

[30] F. Vallée, Phys. Rev. B 49, 2460 (1994).

[31] M. Hase, K. Mizoguchi, H. Harima, S. I. Nakashima, and K. Sakai, Phys. Rev. B 58, 5448 (1998).

[32] M. Hase, K. Ishioka, J. Demsar, K. Ushida, and M. Kitajima, Phys. Rev. B 71, 184301 (2005).